Contingency-Aware Station-Keeping Control of Halo Orbits

Fausto Vega
The Robotics Institute
Carnegie Mellon University
Pittsburgh, PA 15213
fvega@andrew.cmu.edu

Martin Lo
Mission Design & Navigation Section
Jet Propulsion Laboratory
California Institute of Technology
4800 Oak Grove Drive, Pasadena, CA 91109
martin.w.lo@jpl.nasa.gov

Zachary Manchester
The Robotics Institute
Carnegie Mellon University
Pittsburgh, PA 15213
zacm@cmu.edu

Abstract— **We present an algorithm to perform fuel-optimal stationkeeping for spacecraft in unstable halo orbits with additional constraints to ensure safety in the event of a control failure. To enhance safety, we enforce a half-space constraint on the spacecraft trajectory. This constraint biases the trajectory toward the unstable invariant manifold that escapes from the orbit away from the planetary body, reducing the risk of collision. We formulate a convex trajectory-optimization problem to autonomously generate impulsive spacecraft maneuvers to loosely track a halo orbit using a receding-horizon controller. Our solution also provides a safe exit strategy in the event that propulsion is lost at any point in the mission. We validate our algorithm in simulations of the three-body Earth-Moon and Saturn-Enceladus systems, demonstrating both low total delta-v and a safe contingency plan throughout the mission.**

TABLE OF CONTENTS

1. INTRODUCTION

Halo-orbit missions are essential to our understanding of the solar system. Examples of such missions include the James Webb Space Telescope, an infrared telescope orbiting the Sun-Earth L2 libration point to investigate the beginnings of the universe [1], and the Genesis mission, which orbited the Sun-Earth L1 libration point analyzing the solar wind to explore the origins of the solar system [2]. These orbits are periodic, highly unstable, and require several station-keeping maneuvers per orbit to track.

Given the importance and challenges of halo-orbit missions, various station-keeping strategies have been developed over the years to maintain these orbits efficiently. Howell and Pernicka [3] introduced the target-point strategy, which minimizes a weighted cost function that penalizes deviations from the nominal orbit and control effort. However, the timing of the maneuvers is not optimized and the method leads to excessive fuel usage. Gomez, et al. [4] later developed a loose-control station-keeping strategy using dynamical systems theory that removed the unstable component of the invariant manifold along the orbit, but this method does not optimize fuel consumption, a crucial aspect for long-term missions. Maneuver locations are typically predetermined by the mission designer and delta-v is calculated using a differential corrector. For example, the Solar and Heliospheric Observatory (SOHO) mission calculated maneuvers anywhere along the orbit using a differential corrector with the objective of making the x-component of velocity zero at the Sun-Earth line crossing in the rotating frame [5]. Pavlak also uses a single shooting method and compares burning at maximum y amplitudes of the orbit and four predetermined maneuver locations to show that four burns are superior in terms of fuel consumption [6]. However, the major drawback of shooting methods is the high dependence on the initial guess of the free variable along with the formulation of the problem to prevent ill-conditioning [7]. Optimization-based stationkeeping was then introduced by Pavlak by formulating the station-keeping problem as a nonlinear constrained optimization problem with a quadratic objective penalizing fuel consumption [8]. The quadratic objective function is not an accurate measure for fuel consumption which leads to a continuous thrust behavior, excessive fuel consumption, and suboptimal maneuver locations.

Contingency planning is another critical part of space missions. This problem has been explored in the application of spacecraft rendezvous. Specifically, Marsillach uses reachability theory to ensure passive safety in the event of a thrust failure [9]. However, this method is computationally expensive, as these reachable sets need to be calculated for a large portion of the state space. The period of some halo orbits also presents a significant challenge to spacecraft navigation and control. Typically, the navigation process at the Jet Propulsion Laboratory (JPL) requires a minimum of 24 hours to plan and perform a maneuver. However, this time frame is incompatible with some halo orbits that have much shorter periods. For example, an L2 halo orbit in the Saturn-Enceladus system has a period of 16 hours, which is less than the standard maneuver planning window. This mismatch between orbital periods and traditional navigation processes highlights the need for autonomous maneuver planning and execution.

To address these challenges, this paper introduces a method to autonomously optimize impulsive station-keeping maneuvers along the orbit to reduce fuel consumption and provide a safe orbit departure strategy in the event that propulsion is completely lost during the mission. Our contributions include:

- A convex optimization approach for the station-keeping problem that autonomously minimizes fuel consumption, optimizes maneuver locations, and ensures a safe contingency

979-8-3503-5597-0/25/$31.00 ©2025 IEEE

plan in the event of a propulsion failure
• A receding-horizon control algorithm that re-solves for maneuvers twice every orbit to compensate for modeling and state-estimation errors
• Simulation results in the Earth-Moon and Saturn-Enceladus systems demonstrating the effectiveness of our receding-horizon controller.

The paper proceeds as follows: In Section 2 we introduce the circular restricted three-body problem (CR3BP) along with concepts from dynamical-systems theory used in our analysis. Section 3 derives our trajectory optimization formulation and a receding-horizon control strategy. Closed-loop simulation results in two environments presented in Section 4. Finally, Section 5 summarizes our conclusions and directions for future work.

2. BACKGROUND

This section provides a brief review of the CR3BP along with concepts from dynamical systems theory used in our analysis. We refer interested readers to [10] and [11] for more detailed treatments.

The Circular Restricted Three-Body Problem

The CR3BP describes the motion of a small third body in the presence of two larger primary bodies. The two primary masses m_1 and m_2 are assumed to move in circular orbits about their common barycenter, and the third body is assumed to have infinitesimal mass. The mass of m_1 is also assumed to be larger than m_2, and these masses are normalized to unity. The distance between m_1 and m_2 and the rotation speed of m_1 and m_2 about the barycenter are similarly normalized to improve numerical conditioning. To eliminate the time dependence of the dynamics, we use a rotating frame about the barycenter so that the two primary masses are fixed on the x-axis of the rotating frame. In this work, we performed all the analyses using two systems: the Earth-Moon system and the Saturn-Enceladus system.

We augment the CR3BP equations with a normalized thrust (acceleration) input $u = [u_x, u_y, u_z]$. The state of the spacecraft x consists of its position (q_x, q_y, q_z) and velocity (v_x, v_y, v_z) in nondimensionalized units. The controlled continuous CR3BP equations of motion $\dot{x} = f(x,u)$ that describe the state of the spacecraft in the rotating frame are given by (1),

$$\begin{aligned}
\dot{q}_x &= v_x \\
\dot{q}_y &= v_y \\
\dot{q}_z &= v_z \\
\dot{v}_x &= \frac{\partial U}{\partial q_x} + 2v_y + u_x \\
\dot{v}_y &= \frac{\partial U}{\partial q_y} - 2v_x + u_y \\
\dot{v}_z &= \frac{\partial U}{\partial q_z} + u_z
\end{aligned} \tag{1}$$

where U is the augmented potential expressed in (2) and μ is the characteristic mass parameter of the CR3BP.

$$\begin{aligned}
U &= \frac{1}{2}(q_x^2 + q_y^2) + \frac{1-\mu}{r_1} + \frac{\mu}{r_2} \\
r_1 &= [(q_x+\mu)^2 + q_y^2 + q_z^2]^{\frac{1}{2}} \\
r_2 &= [(q_x-1+\mu)^2 + q_y^2 + q_z^2]^{\frac{1}{2}}
\end{aligned} \tag{2}$$

We discretize the continuous dynamics by employing a fourth-order Runge-Kutta integrator, resulting in the discrete-time dynamics model $x_{k+1} = f_d(x_k, u_k)$, where the control input u_k is discretized using a zero-order hold. This model provides the next state of the spacecraft x_{k+1} given a state x_k and a control u_k at the time step k.

Lagrange Points, Periodic Orbits, and Invariant Manifolds

The CR3BP has five equilibrium points, also called "Libration" or "Lagrange" points and commonly numbered L1-L5. The unstable Libration points, L1-L3, are surrounded by low-energy unstable orbits, known as "halo orbits," where very small perturbations lead to large deviations from the orbit. These orbits are useful for mission design, as they maximize observation efficiency [12]. However, halo orbits require satellites to execute frequent station-keeping maneuvers due to instability. We generated an unstable halo orbit about L2 using differential correction with a third-order Richardson expansion as an initial guess [10]; however, obtaining halo orbit initial conditions is also possible via the JPL Solar System Dynamics site [13]. This generated orbit then forms the reference trajectory that the spacecraft tracks.

Along these orbits, there exist sets of low-energy trajectories that escape and approach the periodic orbit, known as invariant manifolds. These manifolds are tube-like structures that are used for various mission-design applications, such as the design of gravity-assist flybys, low-energy capture, and escape around bodies in the solar system. To obtain unstable manifolds, we first calculate the continuous state-transition matrix Φ by integrating the matrix differential equation (3).

$$\begin{aligned}
\dot{\Phi}(t) &= \frac{\partial f}{\partial x}\Phi(t) \\
\Phi(0) &= I
\end{aligned} \tag{3}$$

The state-transition matrix evaluated over one orbit period T is known as the monodromy matrix,

$$M = \Phi(T). \tag{4}$$

An unstable eigenvector of M, which we label v, is locally tangent to the unstable manifold. We use this unstable direction to generate initial conditions for trajectories w on the unstable manifold and then integrate the continuous dynamics $f(x,u)$ forward to time τ using a higher-order integrator. These trajectories are calculated along the halo orbit each at discrete timesteps t_k and their computation is summarized in (5), where ε is a parameter that scales the magnitude of the perturbation in the unstable direction.

$$w(t_k) = \int_0^{\tau} f(x(t_k) \pm \varepsilon\Phi(t_k)v, 0)d\tau \quad t_k \in [0,T] \tag{5}$$

Figure 1 shows example halo orbits to be tracked by our method, along with their unstable manifolds. Adding and subtracting the perturbation $\varepsilon\Phi(t_k)v$ results in both sides of the unstable manifold.

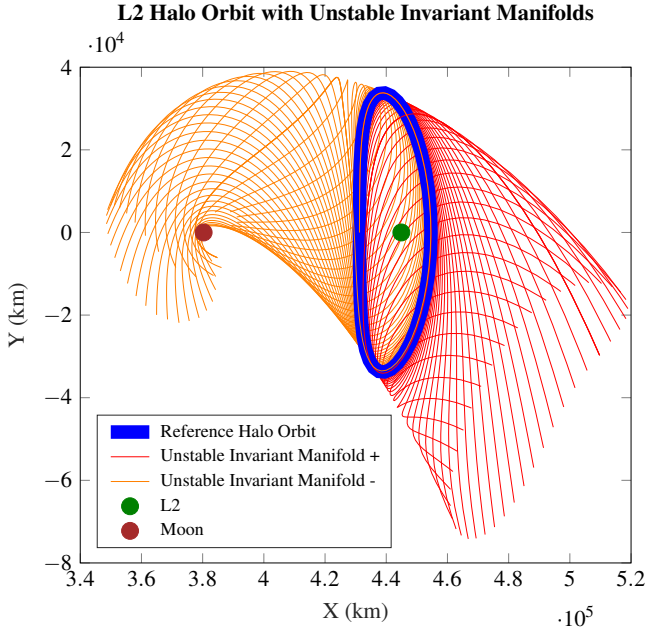

(a) Halo orbit around L2 in the Earth-Moon system with a period of 14.81 days. Adding the perturbation results in the unstable invariant manifold on the right, and subtracting the perturbation leads to the unstable manifold on the left.

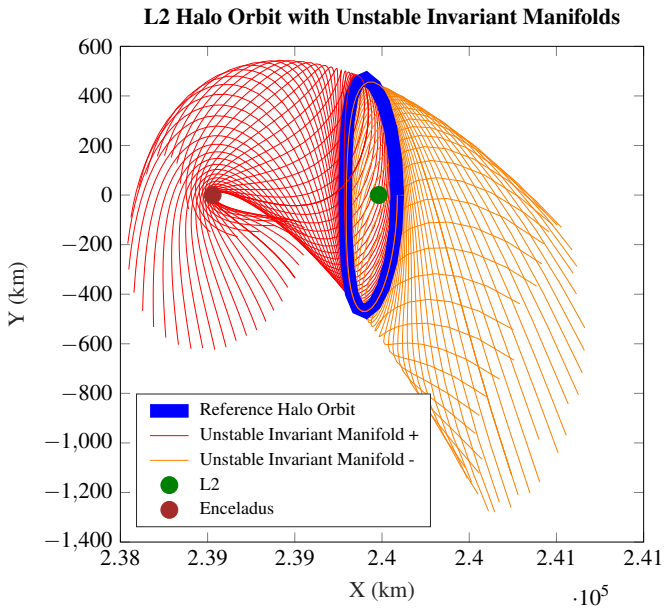

(b) Halo orbit around L2 in the Saturn-Enceladus system with a period of 16.21 hours. Adding the perturbation results in the unstable invariant manifold on the left, and subtracting the perturbation leads to the right unstable manifold

Figure 1: Reference halo orbits in the Earth-Moon and Saturn-Enceladus system along with their unstable invariant manifolds that we use for a safe exit.

3. Optimization-Based Stationkeeping

This section derives our trajectory-optimization formulation and receding-horizon control strategy to solve for fuel optimal stationkeeping maneuvers. We also describe the linearized dynamics used in our convex optimization problem.

Linearized Dynamics

We discretize the reference halo orbit into N knot points. Using a first-order Taylor expansion, we linearize the nonlinear discrete-time dynamics at each knot point $\bar{x}_k$, leading to the linear state-error dynamics:

$$\begin{aligned} \Delta x_{k+1} &\approx A_k \Delta x_k + B_k u_k \\ A_k &= \left.\frac{\partial f_d}{\partial x_k}\right|_{(\bar{x}_k, u_k)} \\ B_k &= \left.\frac{\partial f_d}{\partial u_k}\right|_{(\bar{x}_k, u_k)} \\ \Delta x_k &= x_k - \bar{x}_k \end{aligned} \tag{6}$$

where A_k and B_k are the discrete dynamics Jacobians evaluated at the reference trajectory at timestep k.

Trajectory Optimization

We pose the station-keeping problem as a trajectory optimization problem in (7), where $l_k(x_k, u_k)$ is the stage cost, $l_N(x_k, u_k)$ is the terminal cost, $g(x_k, u_k)$ are the equality constraints and $h(x_k, u_k)$ are the inequality constraints. We solve the problem over a two-orbit horizon $2N$, where N is the number of discrete knot points along the orbit. Convex cost and constraint functions are chosen to guarantee that the solution is globally optimal and can be solved efficiently [14].

$$\begin{aligned} \underset{x_{1:2N}, u_{1:2N-1}}{\text{minimize}} \quad & J = \sum_{k}^{2N-1} l_k(x_k, u_k) + l_N(x_k, u_k) \\ \text{subject to} \quad & g(x_k, u_k) = 0 \\ & h(x_k, u_k) \leq 0 \end{aligned} \tag{7}$$

We focus on minimizing fuel consumption along the orbit while satisfying mission objectives and constraints. The mission objectives include completing a certain number of revolutions around a halo orbit to obtain a large number of observations while minimizing fuel consumption. We chose to minimize the L1 norm of the thrust vector because u_k corresponds directly to delta-v in discrete time, and the sum of delta-v over time approximates the total fuel consumption. The L1 norm also encourages impulsive solutions, which is desired when minimizing fuel [15]:

$$l(x_k, u_k) = ||u_k||_1 \tag{8}$$

Instead of a tracking cost, we employ constraints on maximum state error. Two variants of the state constraint were tested: The first constraint is a Euclidean ball constraint D, which restricts the deviation from the reference trajectory Δx to a user-defined radius as shown in (9). The state radius r consists of the position limit r_q and the velocity limit r_v, which are determined depending on how closely the user wants the satellite to follow the reference trajectory.

This constraint will allow the spacecraft to drift from the reference trajectory and only provide a control impulse when necessary.

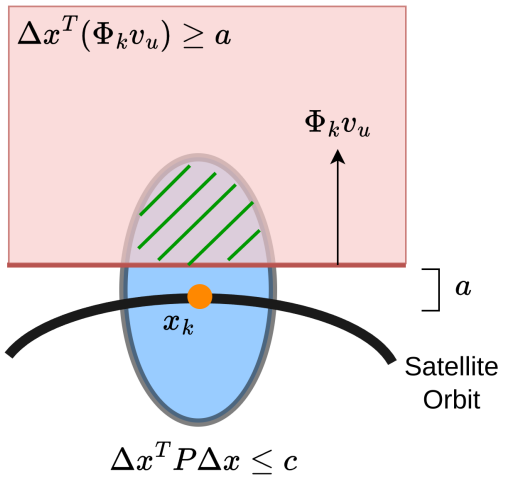

(a) Ellipsoid cost-to-go constraint with the invariant manifold half-space constraint

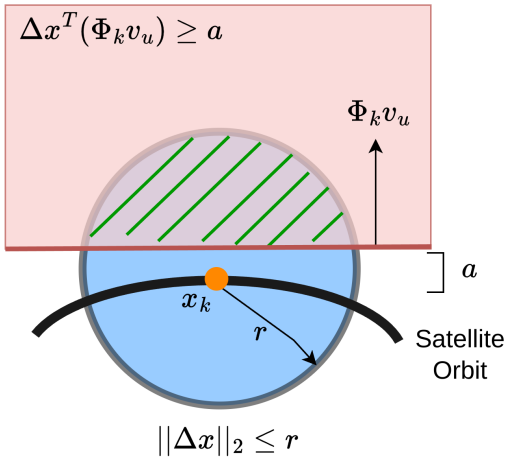

(b) Euclidean ball constraint with the invariant manifold half-space constraint

Figure 2: 2D projection of the state constraints along the orbit x_k. The feasible set is the area intersected with green lines.

$$D(\Delta x_k, r) = \{\Delta x_k \mid ||\Delta x_k||_2 \leq r\}$$
$$r = \begin{bmatrix} r_q \\ r_v \end{bmatrix} \tag{9}$$

The second constraint is an ellipsoid determined by taking a level set of the quadratic cost-to-go function computed by solving a Linear-Quadratic Regulator (LQR) tracking problem. This state constraint is better informed by the dynamics of the problem, therefore we expect better performance compared to the Euclidean-ball constraint. Since the orbit is periodic, the cost-to-go is also periodic for this system [16]. In (10), Q_k and R_k are cost weighting matrices for the states and controls, while Q_N is the terminal cost weighting matrix. The periodic cost-to-go term P_k was calculated by solving the Ricatti recursion until convergence to a periodic solution [17]. In (11), c is a parameter that controls the size of the ellipse.

$$J = \sum_{k=1}^{2N-1} \frac{1}{2} x_k^T Q_k x_k + \frac{1}{2} u_k^T R_k u_k + \frac{1}{2} x_N^T Q_N x_N \tag{10}$$

$$E(\Delta x_k, P_k) = \{\Delta x_k \mid \Delta x_k^T P_k \Delta x_k \leq c\} \tag{11}$$

Next, an initial-state equality constraint is imposed to set the initial delta state to reflect the current observed state of the system x_0.

$$\Delta x_1 = \Delta x_0 \tag{12}$$

Contingency Constraint

Lastly, we impose a half-space constraint H on the state deviation from the reference trajectory Δx_k. This constraint serves as a contingency measure, biasing the trajectory to include a component in the unstable manifold direction. The purpose is to ensure that, in the event of complete propulsion failure, the spacecraft will passively depart the halo orbit away from the planetary body. As demonstrated in [18], any trajectory with a component in the unstable direction will eventually leave the halo through the unstable manifold if no propulsion is applied. This capability allows mission designers to re-plan the mission in safe mode if thrust is regained at a later time, and also prevents collisions with planetary bodies in case of propulsion failures.

The direction of the orbit exit trajectory (either left or right) is generally determined by the sign on v_u, as illustrated in Fig. 5. We assume the half-plane constraint partitions the state space in a way that allows the spacecraft to bias its trajectory toward the unstable manifold that safely exits the halo orbit away from the planetary body. For example, in the Earth-Moon system, the goal is to ensure a safe exit through the right of the L2 point to avoid the Moon, which is located on the left of the L2 point. This contingency constraint provides a local guarantee of a safe exit trajectory when the spacecraft is simulated without propulsion over a short time scale, but may not hold on longer time scales due to the highly nonlinear and chaotic nature of the CR3BP dynamics.

In (13), Φ_k is the state transition matrix at time step k, and multiplying the unstable direction v_u propagates this unstable direction to any time step k. The parameter a in (13) determines the distance of the half-plane from the state x_k which is analogous to ε in (5). A visual representation of the ellipsoidal, Euclidean ball, and half-space constraint is shown in Fig. 2.

$$H(\Delta x_k, \Phi_k) = \{\Delta x_k \mid \Delta x_k^T (\Phi_k v_u) \geq a\} \tag{13}$$

Our full problem formulation is,

$$\begin{aligned} \underset{u_{1:2N-1}}{\text{minimize}} \quad & J = \sum_{k=1}^{2N-1} ||u_k||_1 \\ \text{subject to} \quad & (6),\ (12) \\ & (9) \text{ or } (11),\ (13), \end{aligned} \tag{14}$$

where the equality constraints are the linearized discrete-time error dynamics and initial condition. The inequality constraints consist of a Euclidean ball or ellipsoidal state constraint and an unstable direction half-space constraint.

4. Simulation Experiments

We simulated 100 revolutions around the L2 halo orbit shown in Fig. 1a. The CR3BP dynamics are nondimensionalized by the constants in Table 1. To solve the optimization problem in (14), we use Convex.jl [19], a convex optimization modeling framework in Julia [20], and the Mosek solver [21]. To simulate the nonlinear CR3BP dynamics, we use a higher-order integrator, specifically the Tsitouras-Papakostas 8/7 Runge-Kutta method in DifferentialEquations.jl [22]. To mitigate linearization errors, we implemented a receding-horizon controller that solves the optimization problem in (14) for a two-revolution horizon. We then simulated half of an orbit of optimal controls on the discrete nonlinear dynamics to obtain the new initial state for the next solution. This iterative process is then repeated for the specified mission time. The output of the solver is thrust commands; therefore, we approximate fuel consumption as delta v which is approximated as $u_k \Delta t$. We validate our algorithm in two different settings to assess its efficiency in computing fuel-efficient maneuvers and devising a secure contingency plan in case of losing control. All the simulation code is available on Github[2]

Table 1: Simulation Constants

Constant	Earth-Moon	Saturn-Enceladus
μ	1.215×10^{-2}	1.901×10^{-7}
LU [km]	3.850×10^{5}	2.38529×10^{5}
TU [days]	4.349	0.2189

Earth-Moon Simulation

For this experiment, the initial delta state condition also know as "injection error" was set to 385 m in the x position and 1.856 m/s in the y-component of the velocity. The goal is to loosely follow the orbit from Fig. 1a and ensure a safe departure trajectory throughout the entire mission in the event of an emergency. The halo orbit was discretized into 41 knot points, which resulted in a timestep $\Delta t = 8.911$ hours. First, we compare the fuel consumption between the Euclidean ball and the ellipsoidal constraints. The state weighting matrices Q_k and Q_N for the cost-to-go calculation were set to $1 \times 10^{-3} I(6)$ where $I(6)$ is a 6×6 identity matrix, the control weight matrix R_k was set to $1 \times 10^{3} I(3)$, and $c = 1 \times 10^{4}$ in (11). This cost-to-go metric penalizes control more than state deviation, which matches our fuel consumption objective. For the Euclidean ball constraint, the radius for position r_q and velocity r_v was set to 1000 km and 1000 km/day which will allow the spacecraft to deviate from the reference and only burn when necessary. The constant $a = 1 \times 10^{-2}$ in (13), and this value was tuned to ensure that the manifold constraint was satisfied throughout the entire trajectory. The results of the control inputs for revolutions 10-20 are shown in Fig. 3, where the top plot represents the control with the Euclidean ball constraint and the bottom plot shows the control with the ellipsoid state constraint. For the 100 revolutions, the Euclidean ball constraint consumed 2.89 m/s of fuel while the ellipsoidal constraint used 2.713 m/s. A majority of the fuel is consumed to correct the initial injection error as only 0.357 m/s was consumed for revolutions 2-100 using the Euclidean ball constraint, while the ellipsoid constraint only used 0.0908 m/s for revolutions 2-100.

[2]https://github.com/RoboticExplorationLab/cvx-mpc-stationkeeping

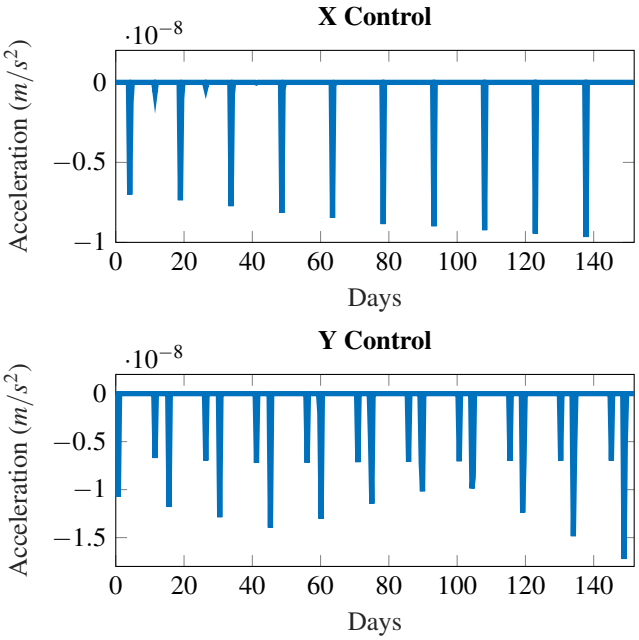

(a) Euclidean ball state constraint control strategy

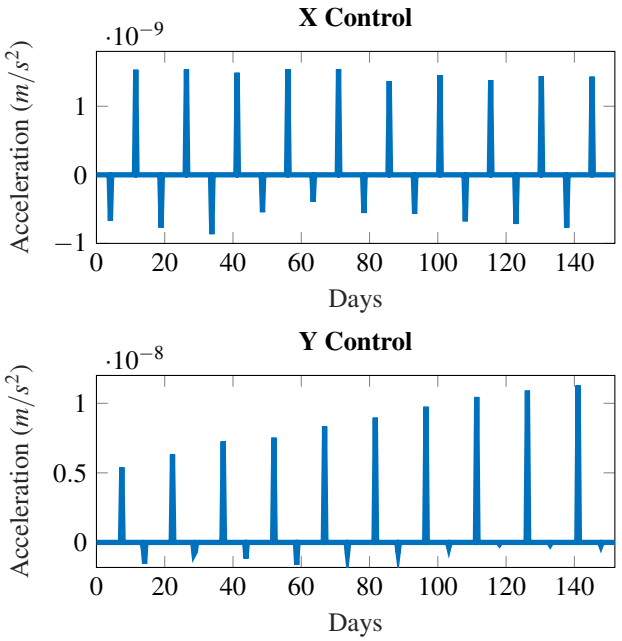

(b) Cost-to-go (ellipsoidal) state constraint control strategy

Figure 3: Comparison of two control strategies for revolutions 10-20 of an L2 halo orbit in the Earth-Moon system. The z control is zero for both strategies.

The total fuel consumption per year is shown in Table 2. As expected, the cost-to-go ellipsoid constraint uses less fuel because the state space is constrained using the LQR cost metric, which heavily penalizes the control effort. The manifold constraint is satisfied throughout the entire 100 revolution trajectory, and to verify that the satellite leaves through the right unstable manifold if the thrusters were to malfunction, we simulate CR3BP dynamics without control forward in time at each state of the solution. As expected, the satellite escapes through the right manifold throughout the mission,

as the optimizer provided station-keeping maneuvers that autonomously biased the trajectory in the unstable manifold direction. However, due to the half-plane assumption in the contingency constraint, there is some transient phase in which the manifold constraint does not guarantee a safe exit over long-horizon simulations. This is because the spacecraft initially executes thrust maneuvers to reduce the effects of the injection error, and then it reaches a steady-state phase where it guarantees a safe exit trajectory locally when close to the reference trajectory. The safe exit trajectory for revolutions 3-100 using the Euclidean ball constraint is shown in Fig. 7a.

We also analyzed the burn locations along the orbit for one of the scenarios. Fig. 4 shows the location of the burns for the control trajectory from the Euclidean ball constraint solution. Interesting patterns emerge, such as the symmetry of the x burns around the y-z plane and the simultaneous x and y burns in the same instance. Both the ellipsoid and Euclidean ball constraints serve as trust regions for the convex problem. Adding the half-space contingency constraint reduces the size of this trust region, ensuring the solution stays close to the halo orbit. Since the dynamics are linearized around the halo orbit, staying near the reference trajectory improves the accuracy of the linear dynamics approximation. This leads to a more accurate solution to the true non-convex problem.

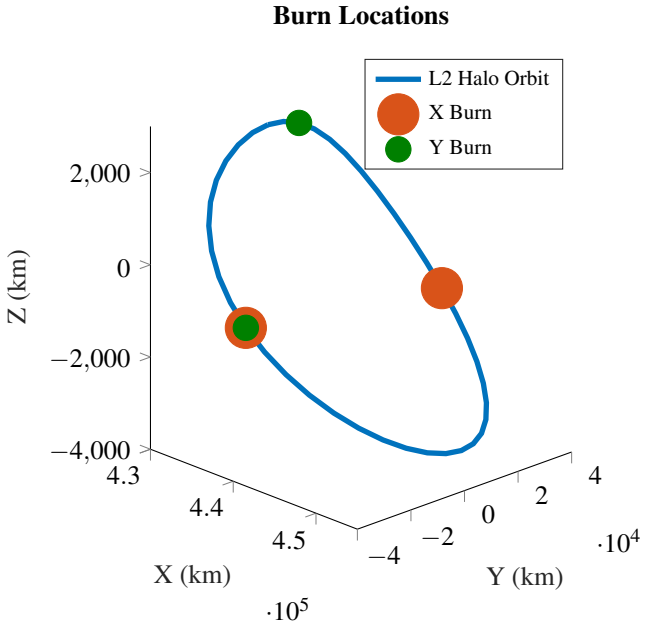

Figure 4: Burn locations for the L2 halo orbit in the Earth Moon system using the Euclidean ball state constraint

Saturn-Enceladus Simulation

For the Saturn-Enceladus system, the initial injection error was set to 238.5 m in the x position and 0.486 m/s in the y-component of the velocity. Similarly, the goal is to track the halo orbit from Fig. 1b with minimal fuel and ensure a safe exit trajectory throughout most of the mission. The L2 halo orbit was discretized to 41 knot points, resulting in a timestep $\Delta t = 24.308$ minutes. The state weighting matrices Q_k and Q_N for the cost-to-go calculation were set to $1 \times 10^{-6} I(6)$, the control weight matrix R_k was set to $1 \times 10^{-3} I(3)$, and $c = 1$ in (11). These values are significantly smaller than those of the Earth-Moon system; however, they were chosen to maintain good numerical stability, and they still penalize the control usage more than the state deviation. For the Euclidean ball constraint, r_q and r_v were set to 100 km and 100 km/day. The constant a was set to 5×10^{-1} in (13). The results of the control inputs for revolutions 10-20 are depicted in Figs. 5 and 6, and the fuel consumption for the Euclidean ball constraint was 5.586 m/s while the ellipsoidal constraint used 5.235 m/s for 100 revolutions.

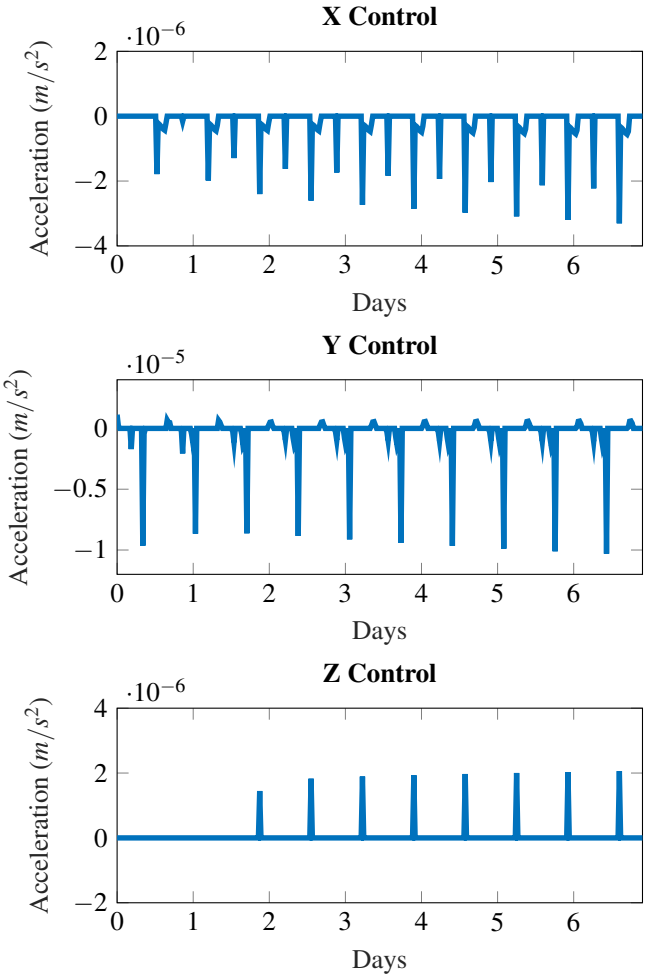

Figure 5: Euclidean ball state constraint control strategy for revolutions 10-20 of an L2 halo orbit in the Saturn-Enceladus system.

The fuel consumption per year is listed in Table 2. Again, the ellipsoidal constraint is superior by a smaller margin, and both constraints provide impulsive burns, which is desired. For the manifold escape trajectory in the Saturn Enceladus system, we simulated the uncontrolled dynamics along all states from the problem using the Euclidean ball constraint solution and the satellite successfully exited through the right unstable manifold for all states in revolutions 12-100 as shown in Fig. 7b. Since the dynamics in the Saturn-Enceladus case are significantly faster than the Earth-Moon, the transient phase lasts for a longer period, however, we still obtain a safe exit trajectory for revolutions 12-100. We obtain a 99.92% success rate in generating safe exit trajectory throughout the entire 100 revolutions in the Earth-Moon system and a 97.53% success rate in the Saturn-Enceladus system. Due to the chaotic nature of the dynamics, a small subset of trajectories in both systems eventually head toward

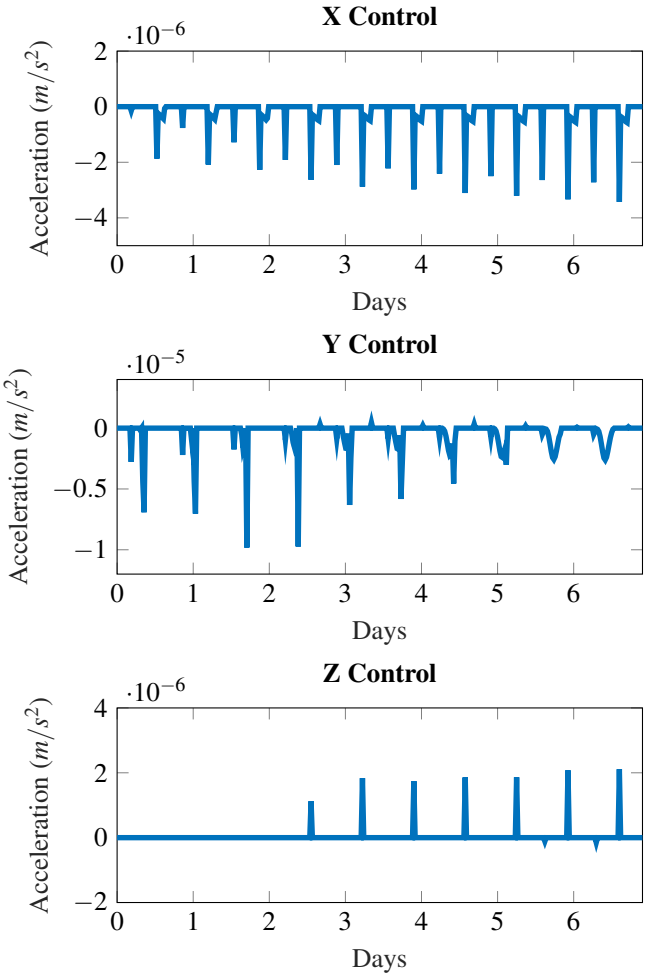

Figure 6: Cost-to-go state (ellipsoidal) constraint control strategy for revolutions 10-20 of an L2 halo orbit in the Saturn-Enceladus system.

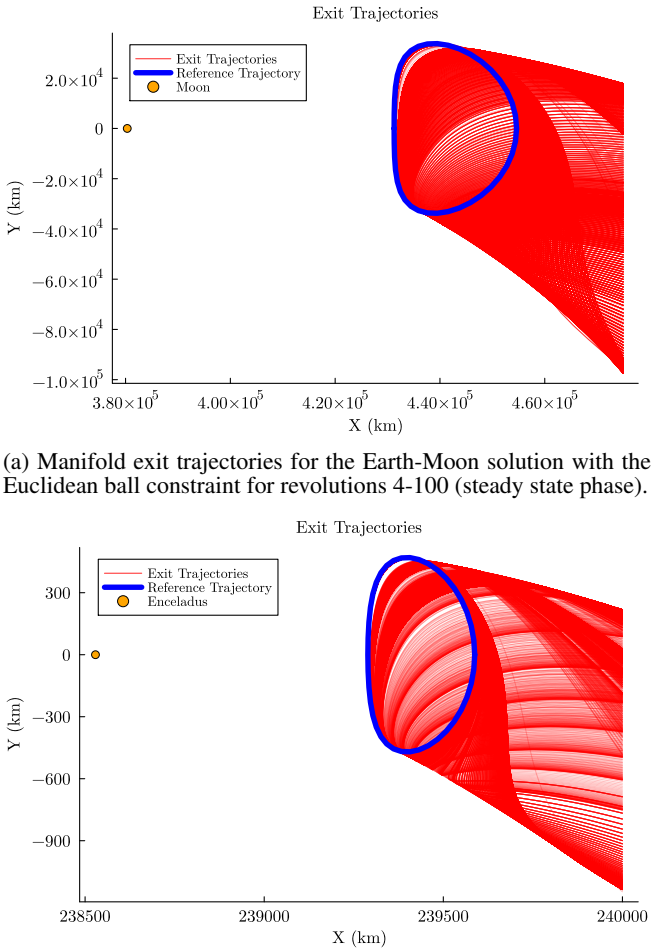

(a) Manifold exit trajectories for the Earth-Moon solution with the Euclidean ball constraint for revolutions 4-100 (steady state phase).

(b) Manifold exit trajectories for the Saturn-Enceladus solution with the Euclidean ball constraint for revolutions 12-100 (steady state phase).

Figure 7: Manifold exit trajectories for the Earth-Moon and Saturn-Enceladus systems.

the planetary body when simulated with no propulsion over a long time-horizon. This happens because the contingency constraint only provides a local guarantee over short time horizons.

Table 2: Fuel Consumption per Year

System	State Constraint	Fuel Consumption $[\frac{m}{s}/yr]$
Earth-Moon	Euclidean Ball	0.712
Earth-Moon	Ellipsoid	0.668
Saturn-Enceladus	Euclidean Ball	30.16
Saturn-Enceladus	Ellipsoid	28.755

5. Conclusions

In this paper, we studied the use of a receding-horizon controller for long-term stationkeeping around an unstable halo orbit that offers a secure contingency plan in the event of thruster malfunctions. The exit strategy is devised by introducing a half-space constraint in the optimization problem to bias the satellite trajectory in a desired direction in the unstable manifold. The controller produces impulsive thrusts at the optimal locations around the orbit and minimizes fuel consumption throughout the desired number of revolutions.

Our future work aims to enhance the robustness of our approach. We plan to simulate the dynamics using a high-fidelity N-body model with ephemeris data. In addition, we plan to incorporate model uncertainties, such as state estimation errors and maneuver execution errors, to develop a robust model-predictive control framework. Another key focus will be exploring various formulations of the contingency constraint, with the goal of achieving 100% safety throughout a 100-revolution mission.

Acknowledgments

This material is based upon work supported by the National Science Foundation under Grand No. DGE2140739. The research was carried out at the Jet Propulsion Laboratory, California Institute of Technology, under a contract with the National Aeronautics and Space Administration (80NM0018D0004). The research was supported in part by the Jet Propulsion Strategic University Research Partnership

Program.

REFERENCES

[1] J. Kalirai, "Scientific discovery with the james webb space telescope," *Contemporary Physics*, vol. 59, no. 3, pp. 251–290, 2018.

[2] M. W. Lo, B. G. Williams, W. E. Bollman, D. Han, Y. Hahn, J. L. Bell, E. A. Hirst, R. A. Corwin, P. E. Hong, K. C. Howell *et al.*, "Genesis mission design," *The Journal of the astronautical sciences*, vol. 49, pp. 169–184, 2001.

[3] K. C. Howell and H. J. Pernicka, "Station-keeping method for libration point trajectories," *Journal of Guidance, Control, and Dynamics*, vol. 16, no. 1, pp. 151–159, 1993.

[4] G. Gómez, J. Llibre, R. Martınez, and C. Simó, "Station keeping of a quasiperiodic halo orbit using invariant manifolds," in *Proceed. 2nd Internat. Symp. on spacecraft flight dynamics, Darmstadt*, 1986, pp. 65–70.

[5] D. W. Dunham and C. E. Roberts, "Stationkeeping techniques for libration-point satellites," *The Journal of the astronautical sciences*, vol. 49, pp. 127–144, 2001.

[6] T. A. Pavlak, "Mission design applications in the earth-moon system: Transfer trajectories and stationkeeping," Ph.D. dissertation, Purdue University, 2010.

[7] D. Folta, N. Bosanac, I. Elliott, L. Mann, R. Mesarch, and J. Rosales, "Astrodynamics convention and modeling reference for lunar, cislunar, and libration point orbits," Tech. Rep., 2022.

[8] T. Pavlak and K. Howell, "Strategy for optimal, long-term stationkeeping of libration point orbits in the earth-moon system," in *AIAA/AAS Astrodynamics Specialist Conference*, 2012, p. 4665.

[9] D. A. Marsillach, S. Di Cairano, U. Kalabić, and A. Weiss, "Fail-safe spacecraft rendezvous on near-rectilinear halo orbits," in *2021 American Control Conference (ACC)*, 2021, pp. 2980–2985.

[10] W. S. Koon, M. W. Lo, J. E. Marsden, and S. D. Ross, "Dynamical systems, the three-body problem and space mission design," in *Equadiff 99: (In 2 Volumes)*. World Scientific, 2000, pp. 1167–1181.

[11] ——, "Heteroclinic connections between periodic orbits and resonance transitions in celestial mechanics," *Chaos: An Interdisciplinary Journal of Nonlinear Science*, vol. 10, no. 2, pp. 427–469, 2000.

[12] F. Bauer, D. Folta, and M. Beckman, "Libration orbit mission design: Applications of numerical & dynamical methods," in *International Conference on Libration Point Orbits and Applications*, 2002.

[13] Jet Propulsion Laboratory. (2024) Periodic Orbits. NASA. [Online]. Available: https://ssd.jpl.nasa.gov/tools/periodic_orbits.html

[14] S. P. Boyd and L. Vandenberghe, *Convex optimization*. Cambridge university press, 2004.

[15] I. Ross, "How to find minimum-fuel controllers," in *AIAA Guidance, Navigation, and Control Conference and Exhibit*, 2004, p. 5346.

[16] S. Bittanti, P. Colaneri, and G. De Nicolao, "The periodic riccati equation," in *The Riccati Equation*. Springer, 1991, pp. 127–162.

[17] R. Tedrake, *Underactuated Robotics*, 2023. [Online]. Available: https://underactuated.csail.mit.edu

[18] F. Vega, M. Lo, Z. Manchester, and J. Sims, "A massively parallel method for fast computation of invariant manifolds."

[19] M. Udell, K. Mohan, D. Zeng, J. Hong, S. Diamond, and S. Boyd, "Convex optimization in julia," in *2014 First Workshop for High Performance Technical Computing in Dynamic Languages*. IEEE, 2014, pp. 18–28.

[20] J. Bezanson, S. Karpinski, V. B. Shah, and A. Edelman, "Julia: A fast dynamic language for technical computing," *arXiv preprint arXiv:1209.5145*, 2012.

[21] M. ApS, "Mosek optimizer api for julia," 2024.

[22] C. Rackauckas and Q. Nie, "DifferentialEquations.jl–a performant and feature-rich ecosystem for solving differential equations in Julia," *Journal of Open Research Software*, vol. 5, no. 1, 2017.

BIOGRAPHY

Fausto Vega *is a PhD student at the Robotics Institute at Carnegie Mellon University (CMU). He received a BS in mechanical engineering from the University of Nevada, Las Vegas and an MS in Robotics at CMU. His research interests include small spacecraft state estimation and optimal control.*

Martin Lo *is a mission designer in the Navigation and Mission Design Section of the Jet Propulsion Laboratory, California Institute of Technology. He has a BS (75) from Caltech and a PhD (80) from Cornell University in mathematics. His specialties are in the three body problem (libration missions using dynamical systems theory) and in constellation design.*

Zac Manchester *is an assistant professor in the Robotics Institute at Carnegie Mellon University and founder of the Robotic Exploration Lab. He received a PhD in aerospace engineering in 2015 and a BS in applied physics in 2009, both from Cornell University. His research interests include control and optimization with applications to aerospace and robotic systems.*